Applied Radiation and Isotopes 94 (2014) 152–157

Contents lists available at ScienceDirect

Applied Radiation and Isotopes

journal homepage: www.elsevier.com/locate/apradiso

Experimental and theoretical investigation of temperature effects on an interbedded betavoltaic employing epitaxial Si and bidirectional ^{63}Ni

Yunpeng Liu, Xiaobin Tang*, Zhiheng Xu, Liang Hong, Da Chen

Department of Nuclear Science and Engineering, Nanjing University of Aeronautics and Astronautics, Nanjing 210016, China

HIGHLIGHTS

- An interbedded betavoltaic based on epitaxial Si and bidirectional ^{63}Ni is presented.
- Electrical performance was measured and calculated at various temperatures.
- Performance temperature dependences of interbedded and monolayer cells are similar.
- Measured V_{oc} temperature dependence is linear as calculated at low temperature.
- Small I_{sc}/I_0 leads to exponential relationship between V_{oc} and T at high temperature.

ARTICLE INFO

Article history:
Received 2 April 2014
Received in revised form
26 June 2014
Accepted 6 August 2014
Available online 24 August 2014

Keywords:
Betavoltaic
Interbedded-structure
Temperature effect
Epitaxial Si
High and low temperature

ABSTRACT

The performance of an interbedded betavoltaic employing epitaxial Si and bidirectional ^{63}Ni was measured and calculated at various temperatures. The experimental results indicate that the temperature dependence of the performance of interbedded betavoltaics is similar to that of monolayer betavoltaics: V_{oc} and P_{max} decrease approximately linearly with increasing temperature at low temperatures of 213.15–253.15 K and decrease exponentially with increasing temperature at high temperatures of 253.15–333.15 K. However, the calculation results indicate that the temperature dependences of V_{oc} and P_{max} are always linear at both high and low temperatures. I_{sc} increases slightly with increasing temperature in both experiment and calculation.

© 2014 Elsevier Ltd. All rights reserved.

1. Introduction

Long-lived, high-energy-density and amenable-to-miniaturization betavoltaics possess great potential for use as next-generation microbatteries in microelectromechanical systems (MEMSs) (Chen et al., 2012). The betavoltaic represents one of the most active and advanced approaches to the development of microbatteries, and has become an intense area of research and development throughout the world (Luo et al., 2011). The depletion region is the core of the betavoltaic, so it is desirable for beta particles to release as much as possible in this region. In previous studies, many PN- or PIN-junction betavoltaics have employed heavily doped substrates — which lead to a narrow space-charge region, a short minority-carrier lifetime, and a consequently low output performance of the cell — or ultra-lightly doped substrates — which result in a high internal resistance of the cell — and ultimately, these betavoltaics cannot satisfy the demands of MEMS applications (Qiao et al., 2011). A concept for a betavoltaic based on an epitaxial Si substrate is demonstrated in this paper. The thin layer of lightly doped epitaxial substrate not only increases the width of the depletion region and the minority-carrier lifetime but also decreases the internal resistance and ultimately improves the electrical performance of the betavoltaic.

A betavoltaic is composed of a beta source and a semiconductor junction energy conversion unit (ECU). The beta-source decay is not affected by the surrounding environment, including the temperature, pressure, and vacuum. However, the characteristics of the ECU, including the minority-carrier lifetime and the reverse saturation current (I_0), can be easily affected by the temperature. Consequently, a change in temperature will influence the output performance of the betavoltaic. Chandrashekhar et al. (2007) have measured the short-circuit current (I_{sc}) and the open-circuit voltage (V_{oc}) of a 4H-SiC betavoltaic irradiated with ^{63}Ni over the room-temperature range from 297.15 K to 359.15 K. Wang et al. (2010) have studied the output performance of a betavoltaic based

* Corresponding author. Tel.: +86 13601582233.
E-mail address: tangxiaobin@nuaa.edu.cn (X. Tang).

http://dx.doi.org/10.1016/j.apradiso.2014.08.011
0969-8043/© 2014 Elsevier Ltd. All rights reserved.

on Si and ^{63}Ni in the temperature range from 233.15 K to 333.15 K. The results of these studies indicated that V_{oc} exhibited a marked linear decrease and I_{sc} increased very little as the temperature increased. Both types of betavoltaics mentioned above employed a monolayer structure, which led to low source-utilization efficiency and low total energy-conversion efficiency. Liu et al. (2014) have studied the *I–V* characteristics of a sandwich betavoltaic based on Si over the room-temperature range and concluded that V_{oc} decreased exponentially and I_{sc} increased very little as temperature increased. In this paper, we fabricated an interbedded-structure betavoltaic employing epitaxial Si and a bidirectional isotope ^{63}Ni. The electrical performance of the interbedded betavoltaic cell was measured and compared with the calculated results in the temperature range 213.15–333.15 K.

2. Materials and methods

2.1. Semiconductor and source materials

Because of their strong radiation hardness, low leakage current, and high theoretical conversion efficiency, third-generation semiconductor materials such as 4H-SiC (Chandrashekhar et al., 2007; Li et al., 2011) and GaN (Olsen, 1993; Honsberg et al., 2005; Lu et al., 2011; Tang et al., 2012b; San et al., 2013) are utilized in many betavoltaic studies. For example, the semiconductor efficiency limit of GaN has been reported to be as high as 28% (Olsen, 1993; Tang et al., 2012b). However, in view of technological maturity and cost, epitaxial Si was used in this paper. Our previous theoretical results demonstrate that the output performance of a betavoltaic with a P-type substrate is superior to that of one with an N-type substrate (Liu et al., 2014). For the experiments conducted in this study, boron-doped homogeneous epitaxial Si with an epitaxial-layer width of 12.5 μm and a crystal orientation of ⟨111⟩ was used. The doped densities of the epitaxial layer and its substrate were 1.2×10^{16} cm^{-3} and 4.9–8.5 $\times 10^{18}$ cm^{-3}, respectively.

The selection of sources is based on half-life, purity, energy density, and end-point energy. Although alpha sources have high energy density, Qiao et al. (2011) have observed that the performance of an Si betavoltaic nearly disappears after 24 h of ^{241}Am irradiation because of radiation damage. Gamma and X-ray sources with strong radioactivity have damaging effects on microcircuits and are difficult to shield. It is recommended that a beta source be used as the energy supply for a betavoltaic. This design will minimize radiation damage. Moreover, beta sources are easy to shield. ^{63}Ni, which emits pure beta particles with moderate energy and has a long half-life, was selected as the energy source for the betavoltaic investigated in this study. A disc-shaped bidirectional isotope source of ^{63}Ni was used, with outside and active diameters of 30 mm and 25 mm, respectively. The activity density of each side was 1.85×10^{8} Bq cm^{-2}.

2.2. Fabrication and measurement

The ECUs for the betavoltaic were manufactured via ion implantation and conventional thermal annealing. The implantation energy and the implantation dose were 120 keV and 3×10^{14} cm^{-2}, respectively. To reduce the tunneling effect, prior to implantation, a layer of SiO_2 of 30 nm in thickness was grown on the front surface of the epitaxial layer via thermal oxidation. After implantation, thermal annealing was performed for a duration of 30 min. Thus, ECUs with a surface doping density of 4.2×10^{19} cm^{-3} and a junction depth of 0.3 μm were successfully produced. The active area of each ECU was 0.5 cm × 0.5 cm.

The back electrode of each ECU was connected to the PCB pad using conductive silver adhesive, and down-leads were attached to the front electrode of each ECU through gold ball bonding. Then, insulated brackets were used to fix the bidirectional ^{63}Ni between the upper and lower ECUs. The upper and lower ECUs individually combined with the ^{63}Ni to form upper and lower monolayer betavoltaics, respectively. Finally, an interbedded epitaxial Si betavoltaic cell was prepared, as illustrated in Fig. 1, by packaging the beta source and the upper and lower ECUs. The upper and lower ECUs were connected in series. In addition, during the loading of the ^{63}Ni, it was possible for the disc-shaped ^{63}Ni slice to touch the down-leads and cause a short circuit or cause a lead to break. To minimize the risk of such problems, a 0.7 mm air gap between the ^{63}Ni and the upper or lower ECU was employed in the experiment.

The effect of temperature on the betavoltaic was investigated using space-environment simulation equipment capable of vacuum and high and low temperatures (KYKY Technology Co., LTD., China, model KYKM800-700), as shown in Fig. 1. The vacuum level of the test chamber was 500 Pa during the measurement. The *I–V* characteristics of the betavoltaics, including the upper monolayer, the low monolayer, and the interbedded cell, were measured in intervals of 10° in the range of 213.15–333.15 K using a Keithley 2636A SourceMeter. In addition, the dark *I–V* characteristics of the ECUs were also measured in the absence of ^{63}Ni irradiation.

2.3. Theoretical calculation

A theoretical calculation mode was established using the actual structural parameters of the interbedded epitaxial Si betavoltaic and the Monte Carlo N-Particle Transport Code, Version 5 (MCNP5). The thickness of the ^{63}Ni source was set to 0.293 μm, and the consequent activity density of one side was 1.85×10^{8} Bq cm^{-2}, as in the case of the experimental ^{63}Ni. In the 0.7 mm gap, the air density was set to 6×10^{-6} g cm^{-3}. The full beta spectrum of ^{63}Ni from ICRP 38 (ICRP, 1983) was employed in the calculation, which is similar to the study reported by Oh et al. (2012). From the simulation of the transport process of beta particles in the semiconductor material, the energy-deposition distribution was obtained at various depths of the ECU. Then, the distribution of the electron–hole pairs (EHPs) in the heavily doped surface region, the depletion region, and the lightly doped epitaxial region was obtained by calculating the ratio of deposited energy with respect to the mean ionization energy. I_{sc} of the betavoltaic was calculated by collecting EHPs. The collection efficiency of EHPs is described in (Honsberg et al., 2005)

$$CE = 1 - \tanh\left(\frac{x}{L}\right) \tag{1}$$

where L is the minority-carrier diffusion length and x is the distance between the position of EHP production and the depletion region. The temperature dependence of L can be expressed as

$$L = \sqrt{\frac{kT}{q} \cdot \mu(N,T) \cdot \tau(N,T)} \tag{2}$$

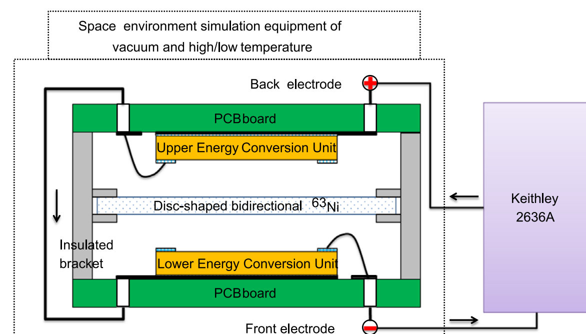

Fig. 1. Measurement schematic for the interbedded epitaxial Si betavoltaic.

Table 1
Parameters used in Eq. (3) (Reggiani et al., 2000).

Parameter	Electrons	Holes
μ_0 (cm^2 V^{-1} s^{-1})	$132.0 \cdot T_n^{-1.3}$	$90.0 \cdot T_n^{-1.3}$
μ_1 (cm^2 V^{-1} s^{-1})	$73.5 \cdot T_n^{-1.25}$	$28.2 \cdot T_n^{-2.0}$
μ_{L0} (cm^2 V^{-1} s^{-1})	1441.0	470.50
C_r (cm^{-3})	$1.22 \times 10^{17} \cdot T_n^{-2.65}$	$1.30 \times 10^{18} \cdot T_n^{-2.2}$
C_s (cm^{-3})	7.00×10^{20}	$1.1 \times 10^{18} \cdot T_n^{-6.2}$
δ	0.72	0.77
c	0.07	0.00
γ	2.45	2.16

Table 2
Parameters used in Eq. (4) (Klaassen, 1992).

Parameter	Electrons	Holes
τ_0 (ms)	2.5	2.5
C_{CRH} (cm^3 s^{-1})	3.00×10^{-13}	1.176×10^{-12}
C_{Aug} cm^3 s^{-1})	1.83×10^{-31}	2.78×10^{-31}
α	1.77	0.57
β	1.18	0.72

where k, T, and q represent the Boltzmann constant, the temperature in Kelvins, and the electric charge in Coulombs; μ and τ are the minority-carrier mobility and the minority-carrier lifetime, respectively; and N is the doping density (N_A or N_D) in the region of interest. The relation between μ and T as a function of the doping density is expressed as follows (Reggiani et al., 2000):

$$\mu(N,T)=\mu_0+\frac{\mu_{L0}T_n^{-\gamma+cT_n}}{1+(N/C_r)^{\delta}}-\frac{\mu_1}{1+(N/C_s)^{-2}} \quad (3)$$

where $T_n = T/300$, μ_{L0} is the value of the lattice mobility at room temperature, and μ_0 and μ_1 represent the minimum values for the carrier mobility at high doping density. The values of the parameters used in Eq. (3) are presented in Table 1.

The temperature dependence of the minority-carrier lifetime can be expressed as follows (Klaassen, 1992):

$$\tau^{-1}(N,T)=(\tau_0^{-1}+C_{SRH}N)T_n^{-\alpha}+(C_{Aug}N^2)T_n^{\beta} \quad (4)$$

where τ_0 is the intrinsic lifetime and C_{SRH} and C_{Aug} are the Shockley–Read–Hall and Auger coefficients, respectively. The values of the parameters used in Eq. (4) are presented in Table 2.

With the aid of MATLAB, other characteristic electrical parameters, including V_{oc} and the maximum output power (P_{max}) of the betavoltaic, were obtained as functions of temperature using the Shockley equation. The specific procedure used to calculate these characteristic electrical parameters was similar to that used in our previous studies (Tang et al., 2012a; Liu et al., 2014).

3. Results

3.1. Dark I-V characteristics

Fig. 2 presents the dark *I–V*characteristics of the upper, lower, and interbedded ECUs at room temperature. At the same bias voltage, the dark current of the interbedded ECUs is lower than that of both the upper and lower ECUs, and that of the upper ECU is the highest. The dark currents of the upper, lower and interbedded ECUs are 3.78×10^{-9} A, 1.02×10^{-9} A, and 1.01×10^{-9} A, respectively, at zero bias and 2.41×10^{-5} A, 3.00×10^{-6} A, and 6.58×10^{-7} A, respectively, at -10 V bias.

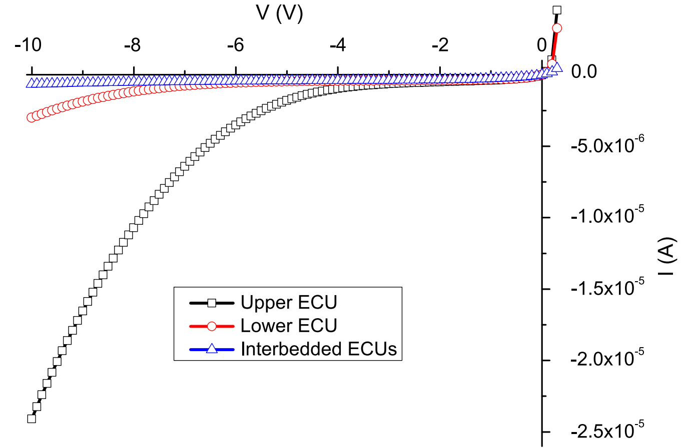

Fig. 2. Dark *I–V* characteristics of upper, lower and interbedded ECUs at 300 K.

3.2. Measured and calculated results

Fig. 3 presents the *I–V* characteristics of the upper, lower and interbedded betavoltaics in the temperature range from 213.15 K to 333.15 K. The trends of the *I–V* curves with increasing temperature for the interbedded betavoltaic are essentially the same as those for the *I–V* curves of the upper and lower betavoltaics. As the temperature increases, the inverse of the slope of the *I–V* curve at the open-circuit voltage point, i.e., the series resistance, gradually decreases, and the inverse of the slope of the *I–V* curve at the short-circuit current point, i.e., the parallel resistance, also gradually decreases.

To display the performance of the betavoltaic in an intuitive manner, the values of V_{oc}, I_{sc}, and P_{max} as functions of temperature were extracted from Fig. 3; these values are presented in Fig. 4. The calculated results for the performance of the interbedded betavoltaic at various temperatures are presented in Fig. 5. Table 3 lists the measured and calculated output performances of the betavoltaics at 213.15 K, 253.15 K, and 333.15 K. The ratio I_{sc}/I_0 of the betavoltaic was determined using

$$V_{oc}=\frac{kT}{q}\ln(I_{sc}/I_0+1) \quad (5)$$

As shown in Fig. 4, the V_{oc}, I_{sc}, and P_{max} values for the interbedded betavoltaic exhibit the same trends as do the corresponding values for the upper and lower betavoltaics. The measured V_{oc} and P_{max} values of these betavoltaics decrease markedly with increasing temperature. The I_{sc} values of these betavoltaics increase slightly as the temperature increases from 213.15 K to 333.15 K. The temperature dependence of the V_{oc} and P_{max} values of these betavoltaics exhibits an approximately linear decline at low temperatures from 213.15 K to 253.15 K and an exponential decrease at high temperatures from 253.15 K to 333.15 K. The V_{oc} sensitivities of the upper, lower, and interbedded betavoltaics are -2.42, -2.94, and -5.24 mV/K, respectively, at low temperature. By contrast, as shown in Fig. 5, the theoretical results indicate that the temperature dependence of V_{oc} and P_{max} for the interbedded betavoltaic should always be linear at both low and high temperatures from 213.15 K to 333.15 K. The theoretical V_{oc} sensitivity for the interbedded betavoltaic is -6.36 mV/K, and for the monolayer betavoltaic, the theoretical V_{oc} sensitivity is -3.18 mV/K. However, I_{sc} exhibits the same trends for the temperature increase from 213.15 K to 333.15 K in both measurement and calculation: I_{sc} increases slightly with increasing temperature.

In addition, as shown in Figs. 3, 4(a), and (b) as well as Table 3, the V_{oc} of the lower betavoltaic is higher than that of the upper betavoltaic at the same temperature. Meanwhile, the V_{oc} of the interbedded betavoltaic is approximately the sum of the

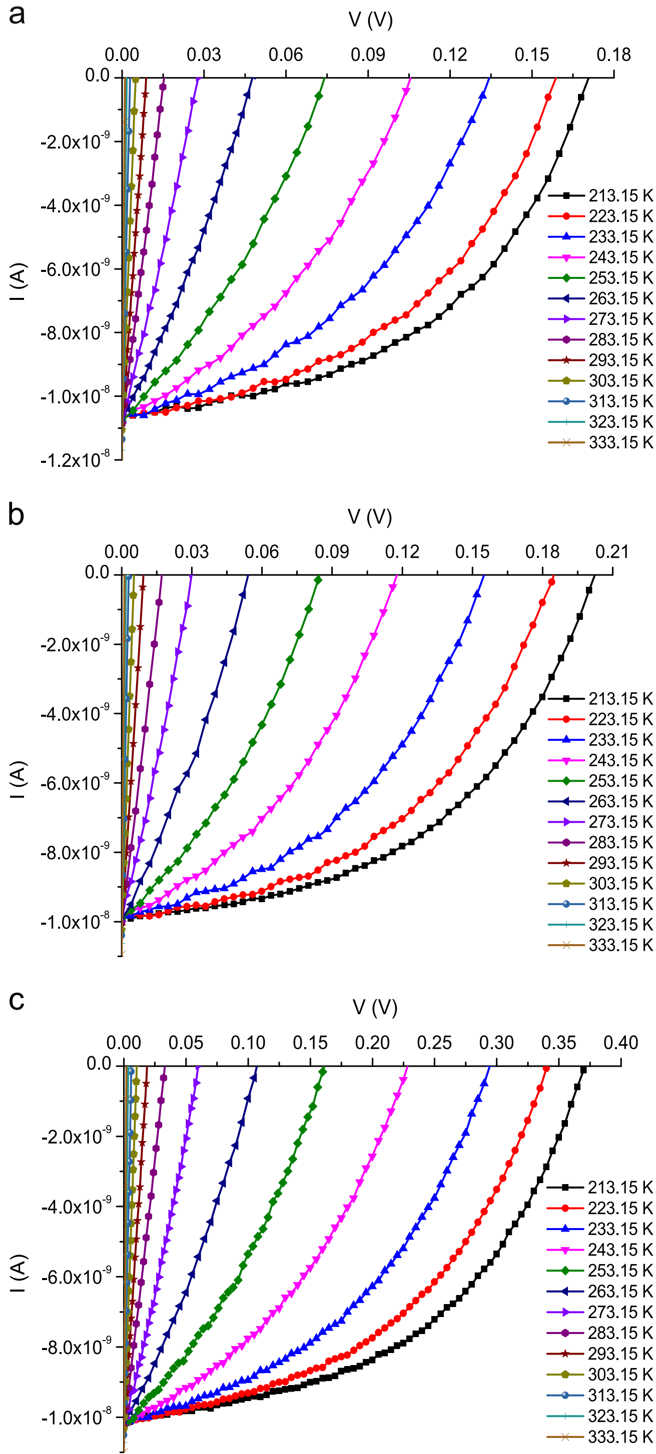

Fig. 3. Measured *I–V* characteristics of the (a) upper, (b) lower, and (c) interbedded betavoltaics at various temperatures.

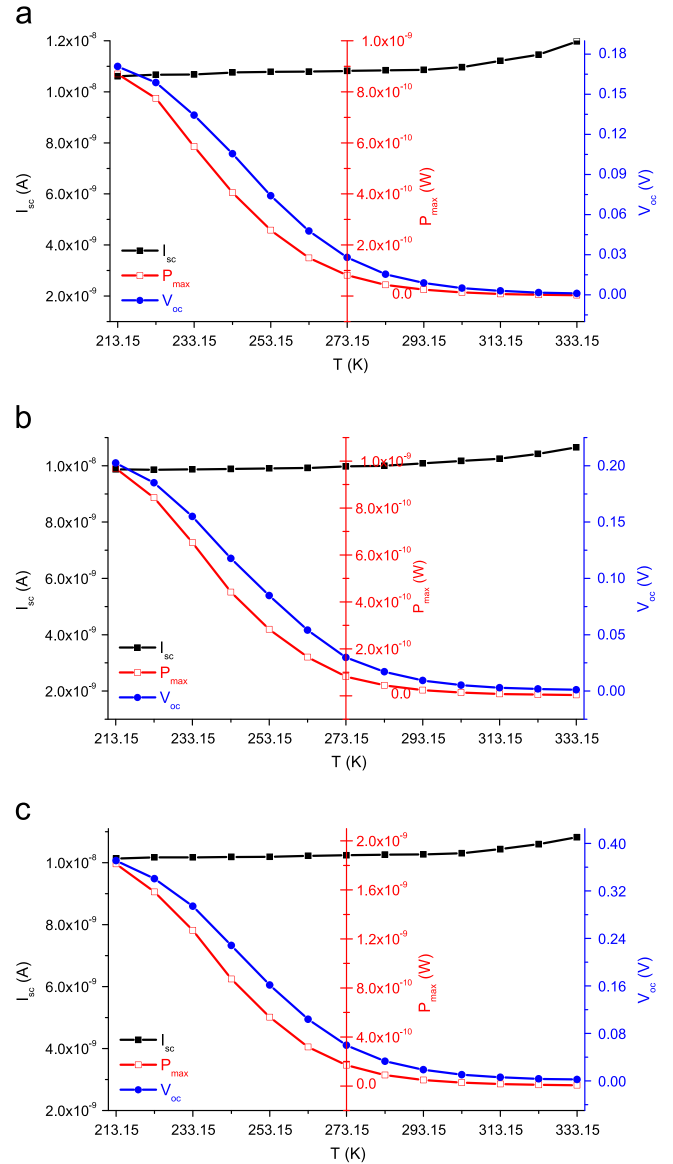

Fig. 4. Measured performances of the (a) upper, (b) lower, and (c) interbedded betavoltaics at various temperatures.

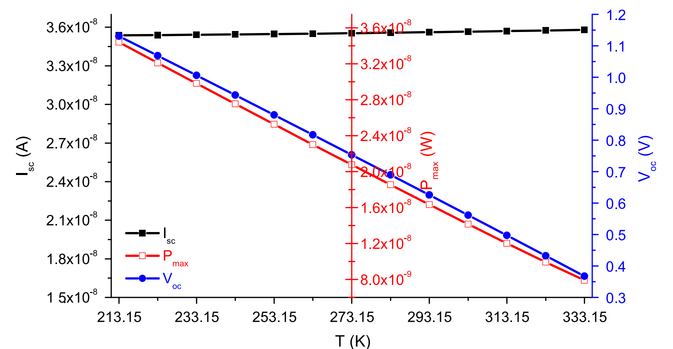

Fig. 5. Calculated performance of the interbedded betavoltaic at various temperatures.

open-circuit voltages of the upper and lower betavoltaics, and I_{sc} remains essentially invariant, as predicted.

4. Discussion

The value of I_{sc} depends on the number and collection efficiency of generated EHPs. On the one hand, the minority-carrier lifetime or the minority-carrier diffusion length has a significant influence on the collection efficiency of EHPs. Long minority-carrier lifetimes and diffusion lengths lead to high collection rates and hence large values of I_{sc}. Wang et al. (2010) have concluded that the minority-carrier lifetime in an ECU is approximately constant in the case of moderate temperature. In our work, the relations between the minority-carrier lifetime and temperature and between the minority-carrier diffusion length and temperature can be obtained

Table 3
Measured and calculated output performances of the betavoltaics at 213.15 K, 253.15 K, and 333.15 K.

Device	T (K)	I_{sc} (A)	V_{oc} (V)	P_{max} (W)	FF	I_{sc}/I_0
Measured upper betavoltaic	213.15	1.061×10^{-8}	0.1707	8.697×10^{-10}	0.480	1.088×10^4
	253.15	1.078×10^{-8}	0.0741	2.580×10^{-10}	0.323	2.885×10^1
	333.15	1.197×10^{-8}	0.0011	3.194×10^{-12}	0.247	3.831×10^{-2}
Measured lower betavoltaic	213.15	9.870×10^{-9}	0.2024	9.691×10^{-10}	0.485	6.096×10^4
	253.15	9.910×10^{-9}	0.0847	2.828×10^{-10}	0.337	4.755×10^1
	333.15	1.065×10^{-8}	0.0012	3.043×10^{-12}	0.247	4.116×10^{-2}
Measured interbedded betavoltaic	213.15	1.013×10^{-8}	0.3710	1.812×10^{-9}	0.482	5.904×10^8
	253.15	1.019×10^{-8}	0.1615	5.604×10^{-10}	0.341	1.637×10^3
	333.15	1.082×10^{-8}	0.0022	5.756×10^{-12}	0.248	7.761×10^{-2}
Calculated interbedded betavoltaic	213.15	3.537×10^{-8}	1.1309	3.340×10^{-8}	0.863	2.341×10^{13}
	253.15	3.547×10^{-8}	0.8801	2.526×10^{-8}	0.815	5.765×10^8
	333.15	3.580×10^{-8}	0.3678	7.898×10^{-9}	0.630	6.046×10^2

from Eqs. (4) and (2), respectively. As illustrated in Fig. 6, the lifetime and the diffusion length of holes in the heavily doped surface region decrease modestly with increasing temperature, and this behavior causes the collection rate to decrease. Because of the recombination rate, the heavily doped surface region contributes little to I_{sc}. Therefore, the temperature behavior of holes in this region has little effect on I_{sc}. EHPs are primarily generated and collected in the lightly doped epitaxial region, where the lifetime and the diffusion length of electrons increase modestly with increasing temperature, causing the collection rate to increase. However, the variation in the lifetime and diffusion length of electrons is small in the temperature range considered in this study (as shown in Fig. 6).

On the other hand, for the specified semiconductor material and beta source, the number of EHPs that are generated is primarily affected by the band gap. The temperature dependences of the band gap (E_g) and the mean ionization energy (ε) can be empirically represented by Eqs. (6) (Li, 2006) and (7) (Klein, 1968), respectively. E_g decreases slightly with increasing temperature, which causes the value of ε to decrease as well. As a consequence, the number of EHPs generated will increase. However, the change in the value of E_g is really very small in this temperature range. For example, E_g decreases from 1.1447 eV to 1.1158 eV as the temperature increases from 213.15 K to 333.15 K, and ε decreases from 3.7052 eV to 3.6242 eV. The percentage decline in E_g between these two temperatures is only 2.52%, and the percentage decline in ε is only 2.18%:

$$E_g = 1.170 - 4.73 \times 10^{-4} T^2/(T + 636) \tag{6}$$

$$\varepsilon = 2.8 E_g + 0.5 \tag{7}$$

Based on the analysis presented above, it can be concluded that the I_{sc} of the betavoltaic increases very little as temperature increases. This conclusion may explain the observed experimental and calculated trends in I_{sc} represented by Figs. 4 and 5.

According to Eq. (5), the V_{oc} value of the betavoltaic primarily depends on the value of I_0. I_0 plays an important role in the performance of the betavoltaic. A small value of I_0 leads to a large value of V_{oc}. I_0 can be expressed as follows:

$$I_0 = Sqn_i^2 (D_p/L_p N_D + D_n/L_n N_A) \tag{8}$$

where the subscripts p and n represent the signs of the holes and electrons in the N and P regions, respectively; S is the area of the PN junction; and n_i is the intrinsic carrier density. The intrinsic carrier density of silicon from 78 K to 340 K is empirically represented by Eq. (9) (Misiakos and Tsamakis, 1993). The value of n_i exhibits an exponential decline with increasing T. According to Eqs. (8) and (9), when the temperature increases, n_i decreases exponentially, which results in a marked decrease in the V_{oc} of the betavoltaic and a consequent decrease in P_{max} and the fill factor (FF) (as shown in Figs. 4, 5, and Table 1):

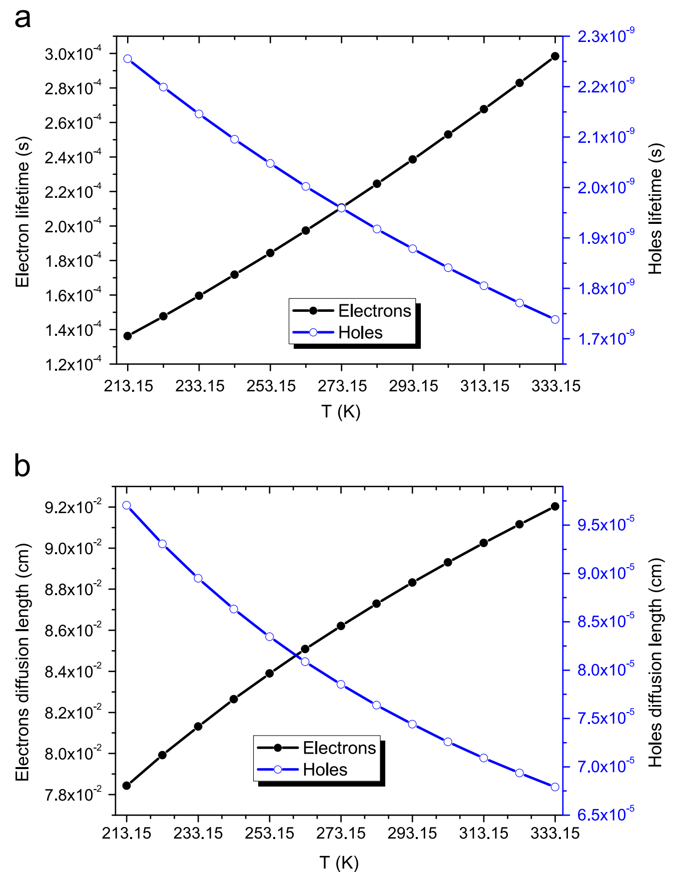

Fig. 6. (a) The minority-carrier lifetime and (b) the minority-carrier diffusion length as functions of temperature.

$$n_i = 5.29 \times 10^{19} (T/300)^{2.54} \exp(-6726/T) \tag{9}$$

The ratio I_{sc}/I_0 directly impacts the variation of V_{oc} with temperature. When I_{sc}/I_0 is large, V_{oc} is a linearly decreasing function of temperature. When the ratio I_{sc}/I_0 is small, V_{oc} is an exponentially decreasing function of temperature (Liu et al., 2014). Ghasemi Nejad et al. (2014) have theoretically investigated the temperature behavior of V_{oc} for various activities of ^{63}Ni. For an ^{63}Ni activity of 3.7×10^4 Bq, it was found that the betavoltaic cannot be used as a temperature sensor for a temperature in excess of 340 K because the low activity of the beta source and the high temperature result in a small value of I_{sc}/I_0, which means that V_{oc} and, consequently, P_{max} decrease nonlinearly with increasing temperature. As shown in Table 3, the experimentally measured

I_{sc}/I_0 ratios of the upper, lower, and interbedded betavoltaics are large at low temperatures from 213.15 K to 253.15 K and small at high temperatures from 253.15 K to 333.15 K. However, the theoretically calculated I_{sc}/I_0 ratios of the interbedded betavoltaic are always large at both low and high temperatures. Therefore, the temperature dependences of V_{oc} and, consequently, P_{max} that were experimentally measured for the betavoltaic differ from those calculated for the betavoltaic.

The conventional thermal annealing process that was employed in the experiment caused significant diffusion of impurities. The shape of the PN junction was undesirable, which led to a high volume recombination rate. In addition, to ensure the direct release of as much energy of the beta particles in the ECU as possible with minimal losses, no passivation technique was performed, which led to a high surface recombination rate. Neither surface recombination nor volume recombination was considered in theoretical calculations; only radiative recombination was taken into account. Therefore, the I_{sc}, the I_{sc}/I_0 ratio, and the resultant V_{oc} and P_{max} that were experimentally measured for the interbedded betavoltaic are all smaller than the theoretically calculated values. Improving the annealing conditions and the surface-treatment procedures, perhaps by employing rapid thermal annealing and passivation techniques, could allow for the development of an ideal abrupt junction and thus decrease I_0, and increase I_{sc}/I_0, V_{oc}, and P_{max}.

5. Conclusion

The fabrication and the operation of an interbedded-structure betavoltaic employing epitaxial Si and bidirectional isotope ^{63}Ni were demonstrated. The electrical performance of the interbedded betavoltaic was measured and compared with the results of theoretical calculations over the temperature range 213.15–333.15 K. The experimental results indicate that the trends of the *I–V* curves of the interbedded and monolayer betavoltaics with increasing temperature are generally similar. The temperature dependence of V_{oc} and P_{max} for the betavoltaic is approximately linear at low temperatures from 213.15 K to 253.15 K and exponential at high temperatures from 253.15 K to 333.15 K. The small value of the ratio I_{sc}/I_0 was used to explain the nonlinearity. The V_{oc} sensitivities of the upper, lower, and interbedded betavoltaics are -2.42, -2.94, and -5.24 mV/K, respectively, at low temperature. By contrast, the results of the theoretical calculation indicate that the V_{oc} and P_{max} values of the interbedded betavoltaic should always decrease linearly with increasing temperature at both high and low temperatures. The theoretically calculated V_{oc} sensitivity is -6.36 mV/K. However, I_{sc} increases slightly as the temperature increases from 213.15 K to 333.15 K in both the experimental measurement and the theoretical calculation. The results of this paper provide an important technical reference for optimization of the design of betavoltaics of this type and for the study of the effects of temperature on their behavior.

Acknowledgments

This work was supported by the National Natural Science Foundation of China (Grant no. 11205088), the Aeronautical Science Foundation of China (Grant no. 2012ZB52021), the Natural Science Foundation of Jiangsu Province (Grant no. BK20141406), the funding of Jiangsu Innovation Program for Graduate Education (Grant no. CXZZ12_0146), and Fundamental Research Funds for the Central Universities.

References

Chandrashekhar, M.V.S., Duggirala, R., Spencer, M.G., Lal, A., 2007. 4H SiC betavoltaic powered temperature transducer. Appl. Phys. Lett. 91 (July (5)) 053511–053511-3.
Chen, C.C., Chang, Y.Y., Zhang, J.W., 2012. A novel betavoltaic microbattery based on swnts thin film-silicon heterojunction. In: 2012 IEEE 25th International Conference on Micro Electro Mechanical Systems (MEMS), January, pp. 1197–1200.
Ghasemi Nejad, G.R., Rahmani, F., Abaeiani, G.R., 2014. Design and optimization of beta-cell temperature sensor based on ^{63}Ni–Si. Appl. Radiat. Isotopes 86, 46–51.
Honsberg, C., Doolittle, W.A., Allen, M., Wang, C., 2005. Gan betavoltaic energy converters. In: Conference Record of the 31st IEEE Photovoltaic Specialists Conference, January 2005, pp. 102–105.
ICRP, 1983. Radionuclide Transformations: Energy and Intensity of Emissions. Technical Report 38, International Commission on Radiological Protection, New York.
Klaassen, D.B.M., 1992. A unified mobility model for device simulation. II. Temperature dependence of carrier mobility and lifetime. Solid-State Electron. 35 (7), 961–967.
Klein, C.A., 1968. Bandgap dependence and related features of radiation ionization energies in semiconductors. J. Appl. Phys. 39 (4), 2029–2038.
Li, S.S., 2006. Semiconductor Physical Electronics, 2nd ed. Springer, New York.
Li, X.Y., Ren, Y., Chen, X.J., Qiao, D.Y., Yuan, W.Z., 2011. ^{63}Ni Schottky barrier nuclear battery of 4H-SiC. J. Radioanal. Nucl. Chem. 287 (1), 173–176.
Liu, Y.P., Tang, X.B., Xu, Z.H., Hong, L., Wang, P., Chen, D., 2014. Optimization and temperature effects on sandwich betavoltaic microbattery. Sci. China Technol. Sci. 57 (1), 14–18.
Lu, M., Zhang, G.G., Fu, K., Yu, G.H., Su, D., Hu, J.F., 2011. Gallium nitride Schottky betavoltaic nuclear batteries. Energy Convers. Manag. 52 (4), 1955–1958.
Luo, S.Z., Wang, G.Q., Zhang, H.M., 2011. Advance in radiation-voltaic isotope battery. J. Isotopes 24 (1), 3–13.
Misiakos, K., Tsamakis, D., 1993. Accurate measurements of the silicon intrinsic carrier density from 78 to 340 K. J. Appl. Phys. 74 (5), 3293–3297.
Oh, K., Prelas, M.A., Rothenberger, J.B., Lukosi, E.D., Rothenberger, J.B., Lukosi, E.D., Montenegro, D., Schott, R.J., Weaver, C.L., Wisniewski, D.A., 2012. Theoretical maximum efficiencies of optimized slab and spherical betavoltaic systems utilizing S-35, Sr-90, and Y-90. Nucl. Technol. 179, 234–242.
Olsen, L.C., 1993. Review of betavoltaic energy conversion. In: NASA Conference Publication. NASA, pp. 256–256.
Qiao, D.Y., Chen, X.J., Ren, Y., Zang, B., Yuan, W.Z., 2011. A nuclear micro-battery based on silicon PIN diode. Acta Phys. Sin. 60 (2), 155–163.
Reggiani, S., Valdinoci, M., Colalongo, L., Rudan, M., Baccarani, G., 2000. An analytical, temperature-dependent model for majority-and minority-carrier mobility in silicon devices. VLSI Des. 10 (4), 467–483.
San, H.S., Yao, S.L., Xiang, W., Cheng, Z.J., Chen, X.Y., 2013. Design and simulation of GaN based schottky betavoltaic nuclear micro-battery. Appl. Radiat. Isotopes 80, 17–22.
Tang, X.B., Ding, D., Liu, Y.P., Chen, D., 2012a. Optimization design and analysis of Si–^{63}Ni betavoltaic battery. Sci. China Technol. Sci. 55 (4), 990–996.
Tang, X.B., Liu, Y.P., Ding, D., Chen, D., 2012b. Optimization design of GaN betavoltaic microbattery. Sci. China Technol. Sci. 55 (3), 659–664.
Wang, G.Q., Rui, H., Wei, H.Y., Zhang, H.M., Yang, Y.Q., Xiong, X.L., Liu, G.P., Luo, S.Z., 2010. The effect of temperature changes on electrical performance of the betavoltaic cell. Appl. Radiat. Isotopes 68 (12), 2214–2217.